SURFACE AND INTERFACE ANALYSIS, VOL. 25, 573–582 (1997)

Waveguide Effect on the Image Formation Process in Near-field Photocurrent Spectroscopy of Semiconductor Laser Diodes

A. Richter, Ch. Lienau* and J. W. Tomm
Max-Born-Institut für Nichtlineare Optik und Kurzzeitspektroskopie, Rudower Chaussee 6, D-12489 Berlin, Germany

Near-field photocurrent spectra of high-power laser diode arrays with different wave-guide characteristics are reported. Subwavelength spatial resolution is achieved by using a near-field fibre probe as the excitation source. The effect of the laser diode waveguide structure and of surface recombination processes on the near-field photocurrent image formation is discussed and analysed in terms of a beam propagation model. Experiments on laser diodes before and after accelerated ageing demonstrate the potential of the technique for analysing microscopic defect formation processes in optoelectronic devices. © **1997 by John Wiley & Sons, Ltd.**

Surf. Interface Anal. **25**, 573–582 (1997)
No. of Figures: 10 No. of Tables: 0 No. of Refs: 19

KEYWORDS: near-field microscopy; laser diodes; photocurrent spectroscopy; optics; semi-conductor lasers

INTRODUCTION

With the increasing growth of the solid-state laser market, the role of high-power laser diode arrays becomes more and more important. Diode arrays are used for a number of applications, such as pumping of solid-state lasers, the generation of blue and UV radiation by frequency doubling and material processing purposes. The high power density in these devices and the high light intensity near their mirror facets cause changes in the structure of the active laser material that ultimately limit the lifetime of the device. Consequently, a microscopic understanding of the ageing processes of high-power laser diodes is of utmost importance for increasing the performance and the lifetime of these devices. This problem has been addressed by a variety of techniques and reviews on this subject have been given by Fukuda[1] and Eliseev.[2] Moreover, from a more fundamental point of view, high-power lasers present unique model systems for studying processes of defect creation and migration.

An understanding of ageing mechanisms in current diode laser arrays is complicated compared to single-emitter diodes by the fact that the properties of the device may vary strongly from emitter to emitter. This is demonstrated in Fig. 1, which shows a spatially resolved photocurrent signal (with a resolution of 30 μm) of a 50 element InAlGaAs laser array for below bandgap excitation at 940 nm before and after 24 h of operation. The non-aged laser diode shows no significant spatial variation of the photocurrent signal between adjacent emitters, which are separated by 200 μm. In contrast, the photocurrent signal of the aged diode fluctuates strongly from emitter to emitter. In particular, two of the 50 emitters of the array show a strongly increased photocurrent signal that is more than double that of the other emitters.

Such observations make the quest for microscopic analysis techniques pertinent. Most recently, near-field photocurrent spectroscopy (NPCS) has been introduced by our group as a new analytical tool for monitoring microscopic ageing processes in high-power laser diodes.[3] In this technique[4–6] the near-field radiation transmitted through a nanometre-sized aperture is used to generate photocarriers that induce a photocurrent inside the sample, acting basically as a photodiode. If the aperture is placed in close proximity to the sample, the excitation spot size is determined by the sub-wavelength size of the aperture and can thus be reduced to below 50 nm. The resolution of the NCPS experiment is determined by the excitation spot size, the absorption length of the radiation and minority carrier transport processes, and could be shown to be better than 250 nm.[4] The technique presents several features that make it particularly attractive for the analysis of laser diodes. It combines high spatial resolution with non-destructiveness and the possibility of resonant excitation by using a tunable-wavelength light source. This allows for the analysis of laser devices at different stages of ageing without affecting the device performance by the analysis process.

In this paper, near-field photocurrent spectra of power laser diode structures with different waveguide characteristics are compared. The image formation process in these experiments is analysed in terms of a ray-tracing model. The role of evanescent and propagating modes, and in particular the influence of infrared active defects and surface recombination processes on the near-field photocurrent spectra, is discussed. Ageing effects on defect concentrations within the active layer are resolved.

The paper is outlined as follows. After a brief description of the experimental set-up, we present macroscopic

* Correspondence to: Ch. Lienau, Max-Born-Institut für Nichtlineare Optik und Kurzzeitspektroskopie, Rudower Chaussee 6, D-12489 Berlin, Germany

CCC 0142–2421/97/070573–10 $17.50

Received 24 October 1996
Accepted 18 February 1997

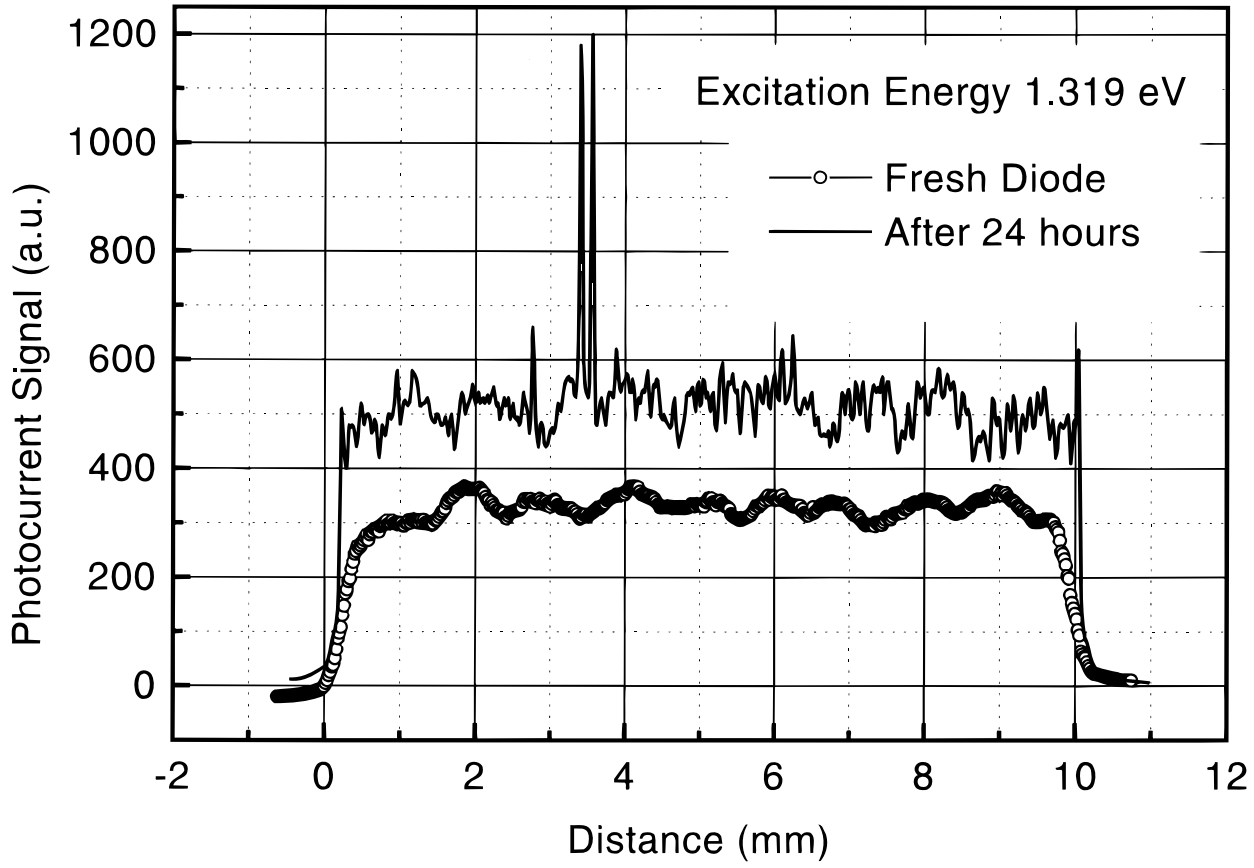

Figure 1. Macroscopic photocurrent linescans at an excitation energy of 1.319 eV (940 nm) of a double quantum well, step index laser diode array consisting of 50 emitters 60 μm wide separated by 140 μm before and after accelerated ageing. While the fresh laser diode shows no significant variation of the photocurrent signal across the diode array, the signal of the aged diode fluctuates strongly from emitter to emitter. In particular, two of the 50 emitters of the array, located at ~3.5 mm, show a photocurrent signal that is more than double that of the other emitters. The spatial resolution in these experiments was ~30 μm.

photocurrent spectra of the investigated structures. Then NPCS experiments obtained for a graded index diode array are analysed and discussed. These results are then compared to experiments performed on a step index array. Finally, the findings are summarized.

EXPERIMENTAL

In the near-field photocurrent experiments, the laser diode is excited by light transmitted through a nanometre-sized aperture at the end of a near-field scanning optional microscopy probe tip.[7] The photoinduced voltage (or current) across the p-i-n junction of the laser diode is then detected as a function of the tip position whilst the laser diode, which is mounted on an *x*-*y*-*z* piezo, is scanned relative to the probe tip (Fig. 2).[4,5] During the scan, the tip-to-sample distance was kept constant at 5 ± 1 nm by using a modified version of the optical shear force set-up proposed in Refs 8 and 9. The shear force mechanism relies on the damping of resonant lateral vibrations of the probe tip as the tip approaches the sample surface to within 10–20 nm. Such resonant lateral vibrations of the probe tip with amplitudes of <10 nm are excited with a dither piezo. The amplitude of the tip vibration is measured by focusing the output of a 670 nm laser diode onto the vibrating tip and imaging the resulting diffraction image onto a quadrant photodiode. The a.c. part of the photodiode signal provides a direct measure of the vibration amplitude and is fed into an electronic feedback system that controls the separation between the tip and the facet of the laser diode by adjusting the *z*-piezo voltage. Therefore, the *z*-piezo voltage gives direct information on the topography of the sample surface. Such shear force images of the *z*-piezo voltage as a function of lateral tip position are recorded simultaneously with the near-field photocurrent images and provide a direct spatial correlation between the near-field photocurrent signal and the layer structure of the laser diode.

The near-field optical microscope used for these experiments is based on a commercial instrument (Topometrix Aurora). Probe tips with a cone angle of 10° were pulled from single-mode optical fibres in a commercial CO_2-laser-based fibre puller (Sutter) and then coated with a 50–100 nm thick aluminium or gold coating. The diameter of the uncoated tips was <30 nm, as was demonstrated by scanning electron microscopy. Shear force images recorded with these uncoated tips gave a lateral resolution of better than 12 nm. The optical resolution of the aluminium- or gold-coated tips was tested using a standard AFM grating and was better than 50 nm. The piezoscanner was software linearized and calibrated against a standard AFM grating with a calibration error of less than $\pm 5\%$. The scan range in these experiments was typically 10×10 μm,[2]

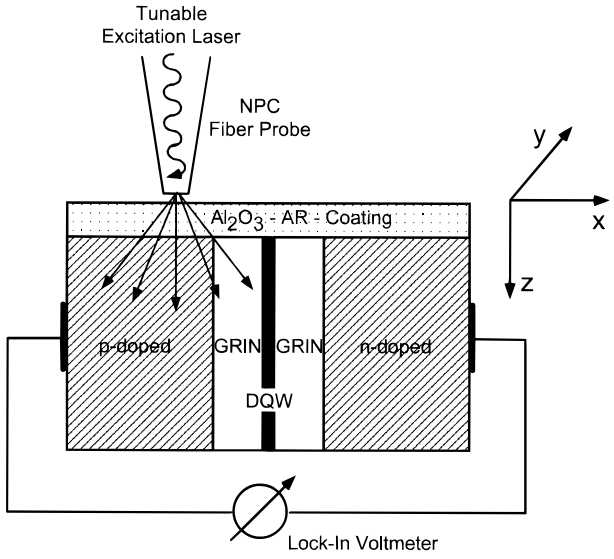

Figure 2. Experimental set-up of the near-field photocurrent (NPC) experiments. In these experiments, the laser diode is excited by tunable continuous-wave laser light transmitted through a nanometre-sized aperture located at the end of a near-field fibre probe. The near-field probe consists of a tapered single-mode optical fibre with a lateral metal coating and aperture diameter of 50–200 nm. The photoinduced voltage (or current) across the p-i-n junction of the laser diode is detected as a function of the tip position whilst the laser diode, which is mounted on an *x*-*y*-*z* piezo, is scanned relative to probe tip. During the scan the tip-to-sample distance was kept constant at 5 ± 1 nm using an optical shear force set-up. The photo-induced signal was detected with a lock-in nanovoltmeter with the laser diode unbiased. The layer structure of the double quantum well, graded index (DQW-GRIN) laser diode array, consisting of two 12 nm GaAs quantum wells surrounded by 220 nm wide undoped $Al_{1-x}Ga_xAs$ ($0.3 < x < 0.6$) graded gap layers and by p- and n-doped 1.5–2 μm thick $Al_{0.6}Ga_{0.4}As$ cladding layers is shown schematically. AR = antireflection.

and 100 × 100 or 200 × 200 data points were recorded for each scan. Tunable continuous-wave laser sources (Cr:LiSAF, Ti:Sapphire) and an HeNe laser were used for excitation. The photoinduced voltage was collected with a lock-in nanovoltmeter at the n- and p-contacts of the unbiased laser diode. The excitation light was amplitude modulated at a frequency of 1 kHz. The power of the excitation light coupled into the fibre probe was ~3 mW and that of the light transmitted through the fibre probe varied between 10 and 100 nW when detected in the far field. At these excitation powers, heating of the fibre tip[10] did not influence the NPCS experiments. The detected photoinduced voltage varied between 1 μV and 1 mV. Macroscopic photocurrent spectra were recorded with a standard optical microscope giving a spatial resolution of 30 μm, a halogen lamp, a monochromator and a lock-in nanovoltmeter.[11]

Two different high-power InAlGaAs/GaAs laser diode array structures were investigated in this work. The layer sequence of both structures has been described earlier in more detail.[12] The first structure is a double quantum well (DQW), graded index separate confinement heterostructure (GRIN-SCH) grown by metalorganic vapour deposition on n-type GaAs substrates. The DQW is situated in a symmetric valley formed by two, 220 nm wide, undoped $Al_{1-x}Ga_xAs$ ($0.3 < x < 0.6$)-graded gap layers. These are surrounded by two, p- and n-doped 1.5–2 μm thick $Al_{0.6}Ga_{0.4}As$ cladding layers with an energy gap (E_g) of ~2.2 eV. The doping profile has its main gradient inside the DQW-GRIN region. The second structure is a step index (SIN) DQW device, where the DQW region is embedded in an undoped 220 nm wide $Al_{0.3}Ga_{0.7}As$ layer ($E_g = 1.8$ eV). In both devices only the contact stripes provide gain guidance and thus form the array structure that was mounted p-side down on a copper heat sink. The front facet reflectivity was adjusted by a 120 nm thick Al_2O_3 layer to ~5%. The photon energy of the laser emission of all devices was determined to be $\hbar\omega = 1.53$ eV ($\lambda = 808$ nm). Accelerated ageing was realized at 20–50 °C for up to 1200 h. The ageing procedure and the changes of the device parameters are discussed in more detail elsewhere.[11]

RESULTS AND DISCUSSION

Macroscopic photocurrent spectra

A macroscopic photocurrent (PC) spectrum (in arbitrary units, full circles) for a fresh DQW-GRIN laser diode emitting at a photon energy of 1.53 eV (808 nm) is depicted in Fig. 3(a). These spectra were measured with a spatial resolution of 30 μm. The calculated spectral shapes of the absorption edge of the DQW $\alpha_{DQW}(\hbar\omega)$ and of the bottom of the GRIN structure $\alpha_{GRIN}(\hbar\omega)$ are added as solid and dotted lines (in cm^{-1}), respectively. In these experiments, the laser array serves as a photodiode that is driven by the incident light at a specific photon energy. The spectral shape of the PC spectrum is closely connected to the absorption coefficient of the entire structure. For all spectral positions, the PC signal magnitude correlates with the sum of the contributions $\sum \alpha_i(\hbar\omega)$ [see Fig. 3(a)] from the different layers (*i*). Furthermore, it depends on the gradient of the sum potential consisting of contributions of the band edges and the doping profile, as well as on the diffusion of the photogenerated carriers into the intrinsic region and, as will be shown below, also on the penetration depth of the excitation light into the laser structure.

Three characteristic contributions to the PC spectrum are resolved. The most prominent feature is the strong signal increase at energies above 1.5 eV, i.e. above the effective bandgap of the DQW structure of 1.53 eV. This evidently arises from the outset of the interband absorption of the transition from the first heavy hole to the first electron sub-band (1hh → 1e) in the DQW (solid line in Fig. 3(a)). The reverse transition is responsible for the laser emission. In the energy range between 1.55 and 1.75 eV, the PC signal intensity remains roughly constant. At energies above 1.75 eV absorption by the graded gap layers sets in (dotted line) and this causes another increase in signal intensity at higher energies.

The third feature in the PC spectrum is the weak broad-band shoulder below the effective band edge (1.53 eV), which extends from energies of 1.5 eV to at least 1.35 eV. Fourier transform PC measurements carried out on these samples revealed that this shoulder extends even further into the infrared, at least down to 0.8 eV.[13] Upon accelerated ageing of the laser device, the PC

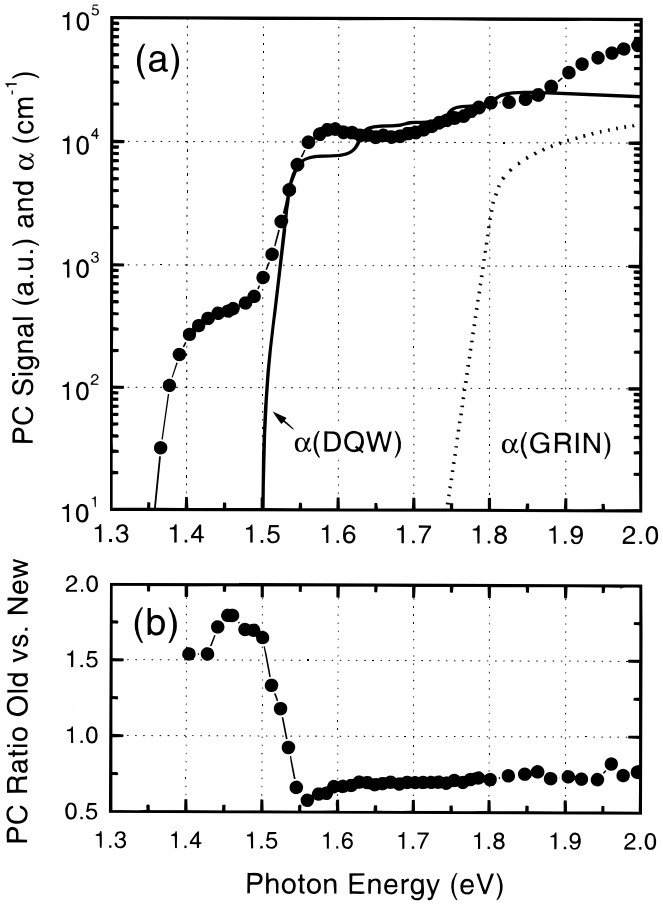

Figure 3. (a) Macroscopic room-temperature photocurrent (PC) spectrum (full circles, in arbitrary units) of a fresh double quantum well, graded index (DQW-GRIN) high-power laser diode with an emission energy of 1.53 eV. Three characteristic features are resolved: a weak below bandgap shoulder at energies between 1.3 and 1.5 eV, which is attributed to defect- or impurity-related absorption; the DQW signal, which dominates the spectrum at energies above 1.55 eV; and absorption by the graded gap layers, which gives rise to an increase of the PC signal at energies above 1.8 eV. The calculated absorption coefficient (cm^{-1}) of the DQW and the bottom of the GRIN region are depicted as a full and a dotted line, respectively. (b) Ratio of the macroscopic PC signals after and before an accelerated ageing test of the DQW-GRIN high-power laser diode. Note the strong increase of the defect-related below bandgap contribution, while the DQW signal of the aged diode at energies above 1.55 eV decreases only slightly.

spectrum changes significantly (see Fig. 3(b)). The PC signal of the below bandgap defect band *increases* by ~75% for energies below 1.5 eV. At energies above 1.55 eV, however, where the PC signal arises predominantly from the interband absorption of the 1hh → 1e DQW transition, the PC signal of the aged diode *decreases* to ~65% of the PC signal of the fresh diode. A transition between signal increase and signal decrease upon ageing is observed in the narrow energy range between 1.5 and 1.55 eV.

The below bandgap contribution to the PC spectrum requires a low-energy absorption mechanism such as defect-band transitions. The energy dependence of the PC spectrum alone does not allow for an unequivocal assignment of the microscopic nature of these transitions. However, one can speculate that ageing of the diode laser enhances the creation and migration of native point defects such as vacancies. Such processes are likely to influence the PC spectra more strongly than the migration of foreign atoms (such as the doping materials) into the active layer. The influence of native defects on the below bandgap absorption is discussed in Refs 14–16. Thus it is very likely that there is a close correlation between laser ageing and point defect creation, and spatially resolved PC experiments should thus give direct insight into ageing-induced microscopic defect formation processes.

Near-field photocurrent spectra

Image formation in the DQW-GRIN laser diodes. In order to understand the *microscopic* origins of the observed changes in the macroscopic PC spectra and to understand the corresponding ageing processes within the laser device, we used a novel technique, namely NPCS, to investigate these diodes. The technique combines the subwavelength resolution of near-field optics with tunable laser excitation and allows for selective investigations of specific parts of the laser device. Two-dimensional NPC scans for a fresh DQW-GRIN laser diode at four selected excitation energies below and above the bandgap are presented in Fig. 4(a). These images have been recorded with fibre probes having an aperture diameter of ~200 nm. The presented images are representative examples of a full set of images recorded at about 20 different spectral positions in the range between 1.44 and 1.96 eV. The scan area is 10 μm × 6 μm and the separation between adjacent data points is 100 nm. In all images, the maximum detected PC has been normalized to unity. In these images, the colour white corresponds to a normalized PC of 1, while black corresponds to zero. The images are shown as recorded without filtering or background correction. A simultaneously recorded shear-force topography of the laser facet is shown in Fig. 4(b). The location of the DQW layer and the n- and p-doped cladding layers is resolved in these images and permits a direct correlation between the NPC image and the layer structure of the laser diode. The alignment of the DQW plane, which is slightly tilted against the scan direction of piezo, is indicated by a solid line. In Fig. 5, cross-sections through these images, without normalization, along a line perpendicular to the DQW plane are related to the laser diode structure. Please note that the data for 1.476 eV have been enhanced by a factor of five. Within experimental error, the integrated intensities in these curves follow the macroscopic PC spectrum of Fig. 3(a). At an excitation energy of 1.476 eV, i.e. for excitation of the below bandgap defect- or impurity-related band, a narrow NPC signal with a width of 700 nm (full width at half-maximum, FWHM) and a maximum in the DQW region is observed. The signal intensity varies only weakly along lines parallel to the DQW plane. At an excitation energy of 1.512 eV, i.e. at the onset of the DQW interband absorption, the signal shape changes drastically into a double maximum structure around the GRIN region and the active region of the laser now appears as a small dip in the centre of this structure. The width of this structure is ~1 μm and the two peaks are separated by 450 nm. At 1.579 eV, i.e. for maximum DQW absorption but no GRIN absorption, we observe a similar double maximum structure with a minimum within the active

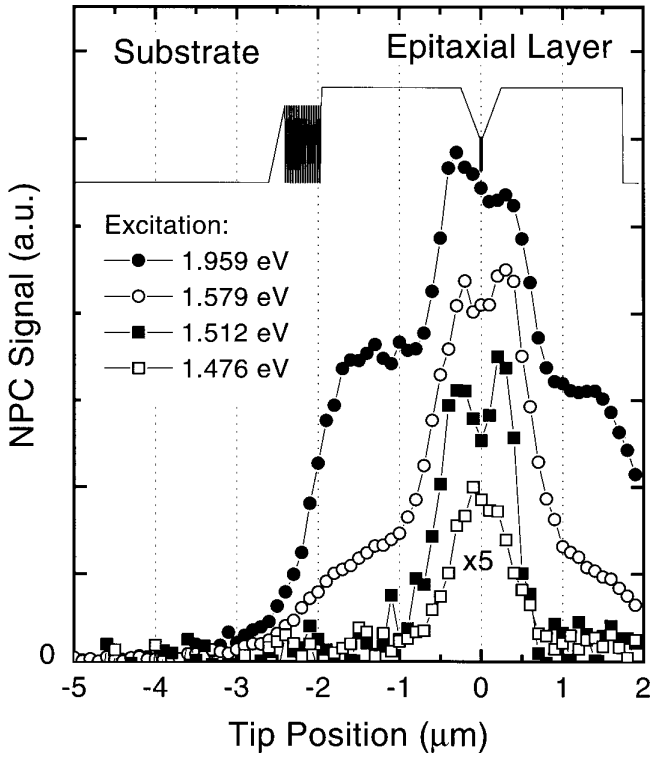

Figure 5. Near-field photocurrent (NPC) linescans at excitation energies of 1.959, 1.579, 1.512 and 1.476 eV of the fresh double quantum well, graded index (DQW-GRIN) laser diode. The scan direction was perpendicular to the active layer. The shape of the conduction band potential is added (solid line).

region, but now with a broad background for tip positions within the cladding layers. At 1.959 eV, i.e. for excitation of the DQW and GRIN transitions, this background increases to ~60% of the maximum NPC signal. The double maximum structure becomes slightly broader than at 1.517 eV and the minimum at the DQW is less pronounced.

To gain an understanding of the microscopic origins of the strongly excitation energy-dependent NPC signals, we analysed the data by simplified two-dimensional beam propagation calculations. Briefly, the excitation light within the device was modelled as a superposition of evanescent and propagating waves and the layer-specific absorption of each of these waves was considered. We assumed that the electric field distribution, which is transmitted through the fibre probe, can be modelled by treating the tip as a one-dimensional slit of width d located along the x-direction. Within the coordinate system introduced in Fig. 2, the x-axis is perpendicular to the DQW plane, located within the y-z-plane. The y-axis points along the mirror facet of the laser and the z-axis is perpendicular to the mirror facet. The electric field directly behind the tip $E(x, z)$ is then approximated as the sum of plane electromagnetic waves

$$E(x, z) \propto \int_{-\infty}^{\infty} \frac{\sin(kx \cdot d/2)}{kx \cdot d/2} \exp[i(kx \cdot x\, kz \cdot z)]\, \mathrm{d}kx \quad (1)$$

where kx and kz denote the components of the wave-vector $k_0 = \sqrt{kx^2 + kz^2} = (2 \cdot \pi \cdot n_i)/\lambda_0$ along the x- and z-directions, respectively. Here, λ_0 is the vacuum wavelength of the excitation light and n_i is the refractive index of the specific layer of the laser structure.

To further simplify the calculations, we assumed in the simulations presented below that interference effects are of minor importance for our experiments, and replaced the sum of plane waves by the sum of optical rays that leave the tip under the direction of their wave vector $\boldsymbol{k} = (kx, kz)$. The relative intensity of each ray is then weighted by the factor $[\sin(kx \cdot d/2)/(kx \cdot d/2)]^2$. These rays are then propagated through the different layers of the diode structure and the absorption within each of these layers gives rise to photogenerated electron–hole pairs that may then induce the PC signal by getting spatially separated. The laser diode is treated as a p-i-n diode and it is initially assumed that all carriers generated within the undoped GRIN and DQW regions contribute to the PC signal with a yield of unity. Electron–hole pairs generated within the surrounding n- or p-doped cladding layers have to diffuse into the region of the potential gradient and therefore the photocurrent yield p_{PC}, i.e. the probability for these carriers to contribute to the PC signal, is taken to decrease exponentially with increasing distance away x from the DQW-GRIN layers

$$P_{PC} = \begin{cases} 1 & \text{if } |x - xgrin| \leqslant 0 \\ \exp(-|x - xgrin|/L) & \text{if } |x - xgrin| > 0 \end{cases} \quad (2)$$

Here, *xgrin* denotes the location of the graded index/cladding layer boundary, and the ambipolar diffusion length is taken as 0.5 μm.

Depending on the magnitude of the x-component of the wave vector kx, we can distinguish between four different kinds of rays:

(1) $|kx| > 2 \cdot \pi \cdot n_{DQW}/\lambda_0$: fully evanescent rays for which kz is imaginary within all layers of the diode and for which, without absorption, the intensity decays exponentially with increasing z;

(2) $2 \cdot \pi \cdot n_{DQW}/\lambda_0 \geqslant |kx| > 2 \cdot \pi \cdot n_{AR}/\lambda_0$, where n_{AR} is the refractive index of the Al_2O_3 antireflection coating: rays that are propagating within the AlGaAs layers but evanescent within the Al_2O_3 coating layer and consequently are exponentially damped in this layer;

(3) $2 \cdot \pi \cdot n_{AR}/\lambda_0 \geqslant |kx| > 2 \cdot \pi \cdot n_{air}/\lambda_0$: evanescent rays in air that are transformed into propagating modes in the Al_2O_3 coating layers;

(4) $2 \cdot \pi \cdot n_{air}/\lambda_0 \geqslant |kx|$: propagating modes in air and the entire laser structure.

The simulations now allow us to study the effect of each class of these rays and thus considerably increase the knowledge about the image formation process in NPCS.

At below bandgap energies, electron–hole pair generation arises only from defect- or impurity-related absorption, while neither the DQW nor the GRIN or doped cladding layers contribute. The impurity distribution is assumed to be homogeneously distributed within the laser structure and the result of a ray-tracing calculation for an impurity absorption coefficient of 10 cm^{-1} is shown in Fig. 6(a). The chosen magnitude of the absorption coefficient is reasonable for typical impurity concentrations of $\sim 10^{16}$–10^{17} cm^{-3} and absorption cross-sections of $\sim 10^{-16}$–10^{-17} cm^2. A variation of the absorption coefficient between 1 and 100 cm^{-1} changes the signal magnitude but affects the

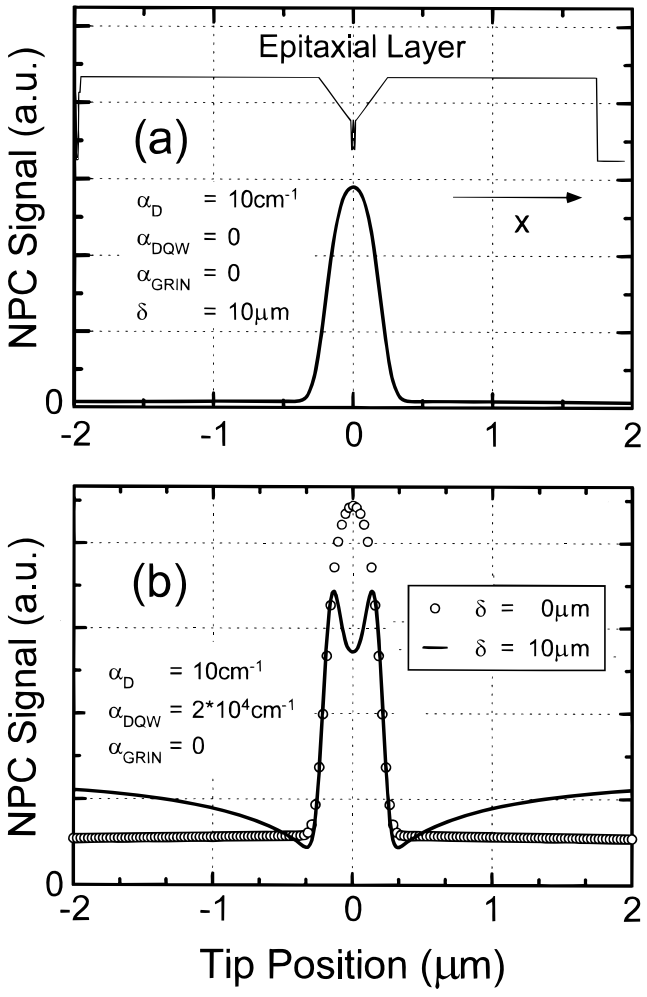

Figure 6. Results of two-dimensional ray-tracing simulations of the near-field photocurrent (NPC) linescans for the double quantum well, graded index (DQW-GRIN) laser diode. The fibre probe is modelled as a one-dimensional slit with a width of 200 nm and both propagating and evanescent modes are considered. Details of the model are described in the text. (a) Below bandgap excitation: an infrared-active impurity- or defect-related site with an absorption coefficient $\alpha_D = 10\ cm^{-1}$ is assumed to be homogeneously distributed within the laser diode. The absorption of both the DQW and the GRIN layers is taken to be negligible. The simulation predicts a narrow peak of the NPC signal inside the DQW region, in agreement with the experimental NPC linescan for $E_{ex} = 1.494$ eV. The signal arises predominantly from guided propagating modes within the DQW-GRIN waveguide structure. (b) Above bandgap excitation: in addition to the defect absorption, an absorption of the active layer with $\alpha_{DQW} = 2 \times 10^4\ cm^{-1}$, corresponding roughly to an excitation energy of 1.579 eV, is considered. The open circles show the result of a simulation neglecting near-surface recombination effects ($\delta = 0$ μm), which predicts a single maximum shape of the NPC linescan. This is in contrast to experiment, e.g. at $E_{ex} = 1.512$ and also at 1.579 eV. A double maximum shape of the linescans is obtained if the photocurrent yield p_{PC} is assumed to decrease near the mirror facet of the laser diode. The solid line was obtained by taking $p_{PC}(z) = 1 - \exp(-z/\delta)$, with $\delta = 10$ μm.

signal shape only weakly. Similar to the experimentally observed NPC linescans at 1.476 eV, the simulations show a narrow NPC signal with a single maximum within the DQW region. From the simulations it follows that the NPC signal is dominated by *propagating* waves *guided* inside the GRIN regions. Rays that enter the DQW or GRIN region of the laser diode under a sufficiently small angle α relative to the z-axis may experience total internal reflection within the graded index region (see Fig. 7). It is important to note that the location along the x-axis, x_r, at which total internal reflection occurs depends both on the entrance angle α and on the x-position x_e at which the rays enter the DQW/GRIN region, because the condition for internal reflection is $n(x_e)\sin(90° - \alpha) = n(x_r)$. These rays thus propagate only within the intrinsic DQW/GRIN region. The contribution of these guided rays to the NPC signal is very different from that of *unguided* rays for which the entrance angle into the DQW/GRIN region is too large to be internally reflected. The guided waves propagate deep into the DQW/GRIN region so that the effective absorption length is much longer than for unguided waves and they thus create a larger amount of carriers inside the p-i-n region. This waveguiding thus directly explains the high spatial resolution of the NPC signal even though the signal is generated by weakly absorbed propagating modes. Because of the small impurity absorption coefficient and their small penetration depth, evanescent modes are of minor importance for the NPC signal at below bandgap energies. The model indicates that their contribution to the signal is at least two orders of magnitude smaller than that of the propagating waves. Due to the strong waveguiding effect, the NPC signals in this diode are also only weakly dependent on minority carrier transport processes.

At excitation energies above 1.5 eV, DQW absorption sets in and the total NPC signal now becomes the sum of a defect-related and a DQW-related contribution. For small DQW absorption coefficients of $< 10^3\ cm^{-1}$, the DQW-related contribution to the NPC signal is again entirely dominated by *propagating* waves *guided* inside the GRIN regions. Within the above model, the shape of the DQW signal is similar to that of the impurity-related signal and shows a narrow peak with a single maximum, located inside the DQW region. With increasing DQW absorption coefficient, i.e. with increasing excess energy of the exciting photons, the amplitude of the DQW-related NPC signal increases whereas the shape remains basically unaffected. For large absorption coefficients, the calculations indicate the onset of a much broader background signal for excitation positions within the n- and p-doped cladding layers. This signal arises predominantly from unguided propagating rays that traverse the DQW region only once. For absorption coefficients above $10^3\ cm^{-1}$, these rays create enough carriers to be detectable in the NPC signal. The amplitude ratio of the contribution from unguided relative to that from guided waves increases with increasing DQW absorption coefficient. This is due to a saturation of the guided wave contribution, because these waves are completely absorbed in the laser diode at high DQW absorption coefficients while the signal caused by the unguided waves increases roughly linearly with increasing absorption coefficient. This increase of the broad background contribution from unguided waves is confirmed experimentally: compare the NPC linescans for excitation energies of 1.579 and 1.512 eV (Fig. 5).

While the growing contribution of background from unguided waves can be consistently explained by our model, the ray-tracing simulations predict that the DQW contribution to the NPC linescans should

possess a single maximum while the experiments for GRIN structure lasers show a pronounced double maximum shape. The ray-tracing simulations showed that this unexpected shape can be attributed to a strong radiationless (near-)surface recombination process. Additional recombination decreases the concentration of excited electron–hole pairs and thus reduces the PC signal.[17] Due to continuous change of the refractive index within the graded gap region, guided rays that are generated with the tip located close to the DQW region experience a stronger wave guiding than those generated further away from the active region. This is schematically shown in Fig. 7 for two rays emitted from the tip under the same angle but for different tip positions. This difference in waveguiding leads to a variation in penetration depth of the guided waves with tip position. Carrier generation thus occurs closer to the surface if the tip is located closer to the DQW region. These carriers are more strongly affected by recombination processes located at the surface and this results in a smaller NPC signal. Phenomenologically, this idea was incorporated into the ray-tracing model by assuming that the photocurrent yield p_{PC}, i.e. the probability with which carriers generated within the DQW/GRIN region contribute to the NPC signal, can be set to zero at the mirror surface ($z = 0$) and increases with increasing distance z as

$$p_{PC} = 1 - \exp(-z/\delta) \quad (3)$$

Results of ray-tracing simulations for a DQW absorption coefficient $\alpha_{DQW} = 2 \times 10^4$ cm^{-1} and a defect absorption coefficient $\alpha_D = 10$ cm^{-1}, including and neglecting near-surface recombination processes, are compared in Fig. 6(b). In the absence of recombination processes ($\delta = 0$ μm, open circles) a single maximum shape is predicted. The solid line shows the linescan obtained for $\delta = 10$ μm, while the other parameters remained unchanged. As expected from the qualitative discussion given above, this strong near-surface recombination now leads to a double maximum shape of the NPC linescan, in agreement with the experimental finding. As in the case of below bandgap excitation energies, the contribution from waves that are evanescent within the laser structure or the Al_2O_3 coating are of minor importance. Non-field photocurrent spectroscopy thus presents a new and direct way to study such near-surface recombination processes.

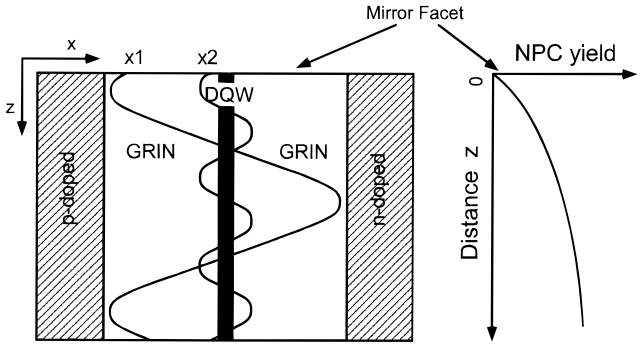

Figure 7. Effect of non-radiative near-surface recombination in graded index (GRIN) structures, illustrated schematically by considering two guided optical rays emitted at different distances from the active double quantum well (DQW) layer. The ray emitted closer to the active layer, at ×2, experiences a stronger guiding and therefore a stronger absorption within the DQW region. Carriers are generated closer to the mirror facet of the laser than for the ray emitted at ×1. In the case of strong near-surface recombination the near-field photocurrent (NPC) yield decreases with decreasing distance z to the mirror facet, and carriers generated by the ray, starting at × 2, thus contribute less to the NPC signal than those generated by the ray emitted at ×1.

At excitation energies above 1.8 eV, absorption by the undoped GRIN layers sets in. The corresponding, relatively large absorption coefficient leads to a strong background signal contribution from unguided propagating waves. The signal intensity of this contribution is practically uniform for all tip positions within the doped cladding layers. This is again in agreement with experiment, as is shown in Fig. 5 in the linescan for an excitation energy of $E_{ex} = 1.959$ eV (solid circles). As absorption by the cladding layers is limited to excitation energies above 2.2 eV, their contribution to the NPC signals can be neglected.

Accelerated ageing of the laser diode has a pronounced effect on the NPC spectra. This is evidenced in Fig. 8, which compares one-dimensional NPC scans along a line perpendicular to the active layer for the DQW-GRIN laser diode before (solid circles) and after (open circles) accelerated ageing. For this comparison we have chosen an excitation energy of 1.531 eV. At this excitation energy, the intensity of the macroscopic PC spectrum (Fig. 2) and thus the integral over the NPC signal along a line perpendicular to the active layer remains unchanged upon ageing. Two pronounced changes of the NPC linescan are noticed. First, the

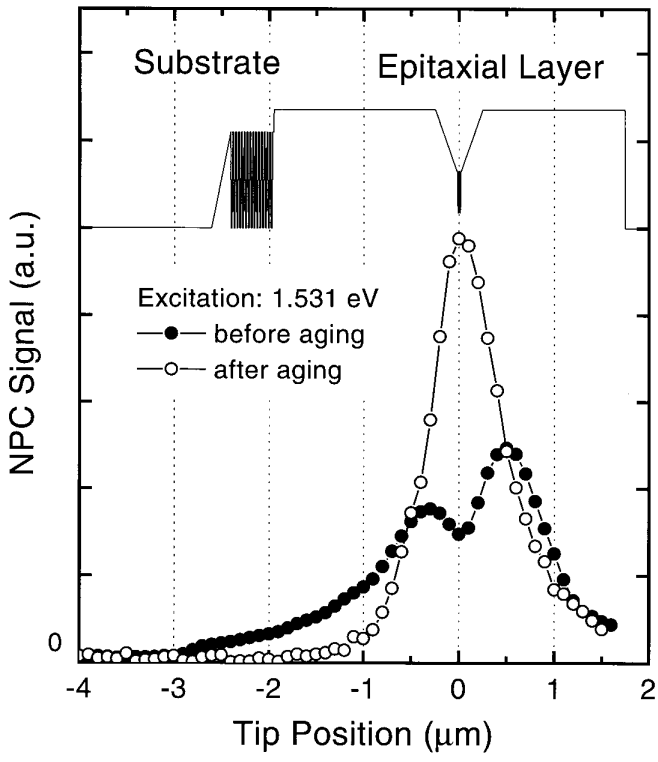

Figure 8. Comparison of near-field photocurrent (NPC) linescans at an excitation energy of 1.531 eV for the double quantum well, graded index (DQW-GRIN) laser diode before (closed circles) and after (open circles) accelerated ageing. At this excitation energy, the intensity of the macroscopic photocurrent spectrum (Fig. 3), corresponding to the integral over the NPC linescan, remains unchanged. The shape of the conduction band potential is added (solid line).

double maximum structure observed for tip positions close to the DQW/GRIN region before ageing changes into a singly peaked structure after ageing. Second, the broad background found in the case of the fresh diode for tip positions within the p-doped cladding layer vanishes. This background was shown before to be related to the absorption of unguided waves within the DQW region. This indicates that the DQW contribution to the NPC signal decreases drastically upon ageing. As it is highly unlikely that the ageing process strongly affects the spectral dependence of the DQW absorption coefficient, we can conclude that this decrease of the DQW-related NPC signal arises from a strong increase of (near-)surface recombination processes. As the overall PC signal does not decrease upon ageing, the decrease of the DQW contribution is compensated by an increase of the defect related contribution. While for the diode before ageing the broader, double maximum DQW contribution dominates the NPC signal at 1.531 eV, the defect-related single maximum contribution becomes dominant upon ageing. This directly explains the unexpected change in the NPC signal from a double maximum into a single maximum structure. The increase in the width of the NPC linescan peak of the aged diode with increasing excess energy from 600 nm at 1.476 eV to 900 nm at 1.531 eV indicates that, in the aged diode, the DQW contribution to the signal at 1.531 eV does not decrease to zero and is large enough to broaden the total NPC signal. A full account of experiments on aged diodes for different excitation wavelengths will be given elsewhere.[18]

Step index (SIN) laser. In this section, the results of the NPCS experiments obtained for the DQW-GRIN diode array are now compared to experiments on a SIN diode array. The layer structure of this array is similar to that of the DQW-GRIN array except for the graded gap waveguide layer, which is replaced by a 220 nm step index $Al_{0.3}Ga_{0.7}As$ layer with an energy gap $E_g = 1.8$ eV. These are surrounded by p- and n-doped 1.5–2 μm thick $Al_{0.6}Ga_{0.4}As$ cladding layers with an energy gap (E_g) of ~2.2 eV. As for the DQW-GRIN structure, the laser emission is at 1.53 eV.

Waveguiding in this SIN structure differs significantly from that in the GRIN structure because the refractive index of the 220 nm SIN layer is constant and total internal reflection can thus only occur at the boundary between the SIN and the surrounding $Al_{0.6}Ga_{0.4}As$ cladding layers (see Fig. 9). The main emphasis of these experiments is to investigate the effect of this difference in waveguiding on the NPC image formation. In particular, it was of interest to check the validity of the ray-tracing approach and to check the conclusions that were drawn on the effect of the radiationless near-surface recombination process on the near-field images. In fresh SIN arrays, the defect-related contribution to the PC is more than an order of magnitude smaller than in the case of the DQW-GRIN diode, which simplifies the separation between defect-related and DQW-related contributions.

The NPC linescans at different excitation energies for a non-aged SIN diode are shown in Fig. 10. These scans are cross-sections through two-dimensional scans along a line perpendicular to the active layer. We note that in these images the maximum of each line-scan was re-

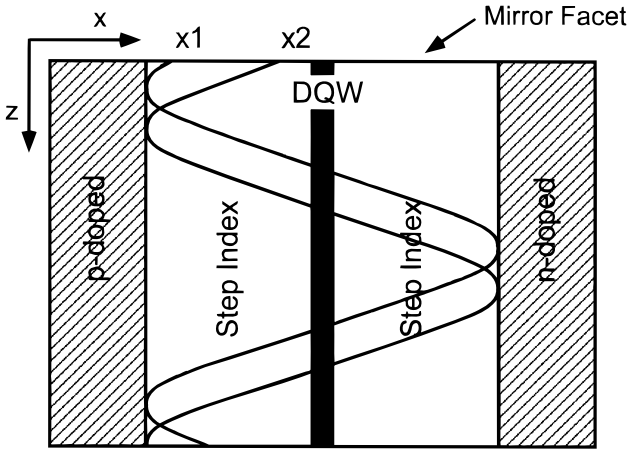

Figure 9. Waveguiding in step index structures illustrated schematically by considering two guided optical rays emitted at different distances from the active double quantum well (DQW) layer. Unlike for the DQW-graded index structure, both rays experience similar waveguiding and are totally internally reflected at the border between the step index and the surrounding cladding layer.

scaled in order to allow for a better comparison between transients at different excitation energies. Within experimental error, the spectral dependence of the signal amplitude of the NPC images follows closely the macroscopic PC spectrum and varies by about three orders of magnitude over the range of excitation energies.

The results obtained for an excitation energy of 1.959 eV, i.e. for excitation well above the band edge of the active layer, are similar to those obtained for the DQW-

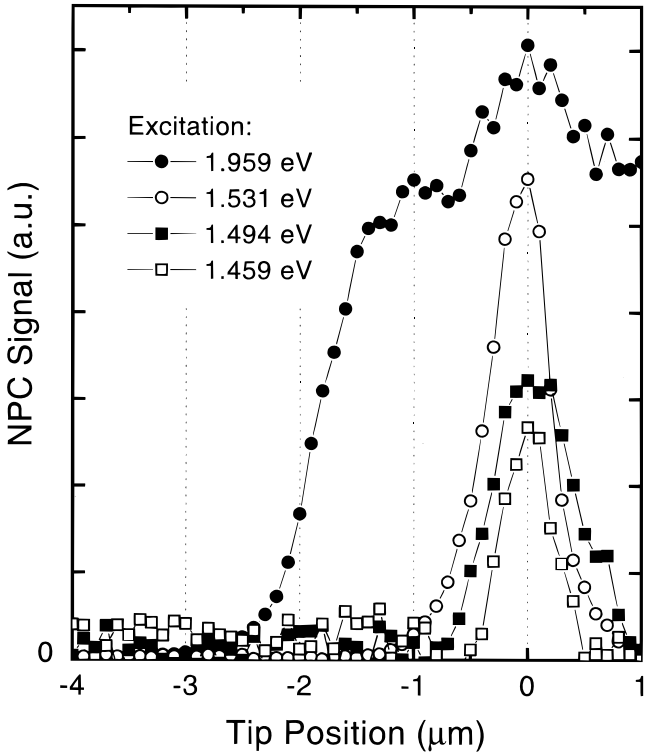

Figure 10. Near-field photocurrent (NPC) linescans at excitation energies of 1.959, 1.531, 1.494 and 1.459 eV of the fresh step index laser diode. The scan direction was perpendicular to the active layer, located at a tip position of 0 μm. The ratio of the NPC intensity at different excitation energies follows closely the macroscopic photocurrent spectrum.

GRIN structure. The signal consists again of a broad plateau for tip positions inside the p- and n-doped cladding layer and a smaller peak located within the SIN waveguide layer. The plateau can be attributed to absorption of unguided propagating waves within the DQW and SIN layers, while the smaller peak is mainly related to the absorption of guided propagating waves within the DQW layer.

For excitation energies below the effective bandgap of the active layer, i.e. at $E_{ex} = 1.459$ eV and $E_{ex} = 1.494$ eV, a narrow structure with a single peak inside the centre of the waveguide structure is found. These signals are similar to that for the DQW-GRIN diode and can again be assigned to an infrared active defect- or impurity-related contribution. The width of the signal varies between 600 and 700 nm. The signal shape can be reproduced qualitatively within the ray-tracing model introduced above if a small defect-related absorption coefficient on the order of 1 cm^{-1} is assumed to be homogenously distributed within the laser device. Here, the NPC signal is entirely due to the absorption of propagating waves guided within the SIN structure and the signal shape is due to waveguiding effects while minority carrier transport is of minor importance. The role of evanescent modes is negligible.

The NPC signal intensity of the fresh diode increases by about a factor of 20 as the excitation energy is increased from 1.494 to 1.531 eV. This is due to the onset of DQW absorption, which dominates the NPC signal at $E_x = 1.531$ eV. Unlike for the DQW-GRIN diode, the shape of the NPC signal does *not* change drastically at the onset of DQW absorption. The NPC signal still shows a *single* maximum shape with its peak located at the centre of the waveguide structure. The width of the NPC signal is $\sim$600–650 nm. This singly peaked shape has to be compared to the pronounced double maximum feature of the fresh GRIN structure. Within the ray-tracing model introduced above, this change in the signal from a double maximum into a single maximum shape upon changing of the waveguide layer from a GRIN into a SIN structure is readily explained. Consider again two guided rays emitted from a point-like source within the SIN layer. As in Fig. 6, the rays are assumed to be emitted under the same angle but for different tip positions relative to the active layer. As the refractive index profile is constant within the SIN, both rays are now totally reflected at the boundary between the SIN and the surrounding cladding layer. Therefore, for the SIN structure, both rays experience the same guiding and consequently also the same absorption by the active DQW layer. Unlike for the GRIN structure, the penetration depth of the rays is *not* dependent on the tip position. Even in the case of strong near-surface recombination processes, the PC yield does not depend on the tip location and this explains why the shape of the NPC signals does not change at the onset of strong DQW absorption.

We can conclude that the introduced ray-tracing model allows the NPC signals to be explained qualitatively for both the GRIN and the SIN structures, and that indeed the waveguiding characteristics of the diode layers have a particularly strong influence on the NPC image formation process. This provides additional evidence for the importance of propagating guided beams for the NPC signals. In SIN structures, due to the insensitivity of the waveguide properties to the exact location of the excitation source within the wave-guide layer, (near-)surface recombination effects have only a minor effect on the shape of the NPC images.

SUMMARY AND CONCLUSION

In this paper we present a comparative study of spatially resolved NPC spectra of two high-power laser diode arrays with different waveguide characteristics. In these experiments subwavelength spatial resolution was demonstrated by exciting the laser device through a nanometre-sized aperture located at the end of a near-field fibre probe. Tuning of the excitation energy across the bandgap energy of the laser allowed us to study specific components of the laser device experiments. At below bandgap energies carrier generation is dominated by absorption of an infrared active defect- or impurity-related site, while at energies above the laser emission at 1.53 eV, absorption of the active DQW layer dominates. In the DQW-GRIN diode array, a strong variation of the shape of the NPC images with excitation energy was observed. In particular, the DQW-related NPC signal showed a pronounced double maximum structure. With the help of a ray-tracing model, the NPC image contrast was found to arise predominantly from propagating waves guided within the graded gap layer and the observed double maximum was assigned to arise from (near-)surface radiationless recombination effects. The lineshape of the near-field scans was shown to depend strongly on the magnitude of the surface recombination velocity so that NPCS presents a powerful tool for the microscopic analysis of ageing effects on surface recombination processes.

The conclusions drawn from the study of the DQW-GRIN structure were strongly supported by a comparative study of a diode laser array of a similar composition, except for a different (step index) waveguide structure. The change in waveguide structure makes the shape of the NPC images less sensitive to surface recombination processes so that in this structure the ageing procedure mainly affects the magnitude of the NPC signals.

So far, our discussion has not clarified the nature of the defect observed in the NPC experiments. We pointed out that native infrared active defects contribute to the below bandgap PC signal. These defects are known to be readily observable in DLTS spectra[19] and such measurements are currently under way. We note, however, that due to the dominance of waveguiding effects on the NPC image formation process, the current experiments can also be explained by the migration of impurity-related defects into the waveguide layer. This will be the subject of further investigations.

In summary, we demonstrated that NPCS has the potential to provide direct insight into the microscopic processes of ageing-induced defect creation and surface recombination in the active region of high-power laser diodes.

Acknowledgements

The authors would like to thank A. Bärwolff and U. Menzel for helpful discussions, Ch. Lier for expert technical assistance and G.

Behme for help in preparing some of the figures. Special thanks are due to F. X. Daiminger from Jenoptik Laserdiode GmbH and J. Luft from Siemens AG for providing us with the high-quality laser diode samples. In particular, we wish to thank T. Elsaesser for careful reading of the manuscript and continuous support of this work.

REFERENCES

1. M. Fukuda, in *Reliability and Degradation of Semiconductor Lasers and LEDs*. Artech House Inc., Boston (1991).
2. P. G. Eliseev, in *Reliability Problems of Semiconductor Lasers*. Nova Science Publishers, Commack (1991).
3. A. Richter, J. W. Tomm, Ch. Lienau and J. Luft, *Appl. Phys. Lett.* **69**, 3981 (1996).
4. S. K. Buratto, J. W. P. Hsu, E. Betzig, J. K. Trautman, R. B. Bylsma, C. C. Bahr and M. J. Cardillo, *Appl. Phys. Lett.* **65**, 2654 (1994).
5. M. S. Ünlü, B. B. Goldberg, W. D. Herzog, D. Sun and E. Towe, *Appl. Phys. Lett.* **67**, 1862 (1995).
6. B. B. Goldberg, M. S. Ünlü, W. D. Herzog, H. F. Ghaemi and E. Towe, *IEEE J. Select. Topics Quant. Electron.* **1**, 1073 (1995).
7. E. Betzig, J. K. Trautman, T. D. Harris, J. S. Weiner and R. L. Kostelak, *Science* **251**, 1468 (1991).
8. E. Betzig, P. L. Finn and J. S. Weiner, *Appl. Phys. Lett.* **60**, 2484 (1992).
9. P. C. Yang, Y. Chen and M. Vaez-Irvani, *J. Appl. Phys.* **71**, 2499 (1992).
10. Ch. Lienau, A. Richter and Th. Elsaesser, *Appl. Phys. Lett.* **69**, 325 (1996).
11. J. W. Tomm, A. Bärwolff, U. Menzel, M. Voß; R. Puchert, Th. Elsaesser, F. X. Daiminger, S. Heinemann and J. Luft, *J. Appl. Phys.* **81**, 2059 (1997).
12. M. Voss, C. Lier, U. Menzel, A. Bärwolff and T. Elsaesser, *J. Appl. Phys.* **79**, 1170 (1996).
13. J. W. Tomm, A. Bärwolff, A. Gerhard and J. Donnecker, unpublished.
14. G. M. Martin, *Appl. Phys. Lett.* **39**, 747 (1981).
15. S. Tüzemen and M. R. Brozel, *Appl. Surf. Sci.* **50**, 395 (1991).
16. K. Saarinen, S. Kuisma, P. Hautojärvi, C. Corbel and C. LeBerre, *Phys. Rev. Lett.* **70**, 2794 (1993).
17. H. J. Leamy, *J. Appl. Phys.* **53**, R51 (1982).
18. Ch. Lienau, A. Richter and J. W. Tomm, *Applied Phys. A* **64**, 341 (1997).
19. J. Lagowski, D. G. Lin, T. P. Chen, M. Skowronski and H. C. Gatos, *Appl. Phys. Lett.* **47**, 929 (1985).

